Yukutake *et al. Earth, Planets and Space* (2017) 69:164
https://doi.org/10.1186/s40623-017-0751-y

Earth, Planets and Space

FULL PAPER

Open Access

Analyzing the continuous volcanic tremors detected during the 2015 phreatic eruption of the Hakone volcano

Yohei Yukutake[1*], Ryou Honda[1], Masatake Harada[1], Ryosuke Doke[1], Tatsuhiko Saito[2], Tomotake Ueno[2], Shin'ichi Sakai[3] and Yuichi Morita[3]

Abstract

In the present study, we analyze the seismic signals from a continuous volcanic tremor that occurred during a small phreatic eruption of the Hakone volcano, in the Owakudani geothermal region of central Japan, on June 29, 2015. The signals were detected for 2 days, from June 29 to July 1, at stations near the vents. The frequency component of the volcanic tremors showed a broad peak within 1–6 Hz. The characteristics of the frequency component did not vary with time and were independent of the amplitude of the tremor. The largest amplitude was observed at the end of the tremor activity, 2 days after the onset of the eruption. We estimated the location of the source using a cross-correlation analysis of waveform envelopes. The locations of volcanic tremors are determined near the vents of eruption and the surface, with the area of the upper extent of an open crack estimated using changes in the tilt. The duration-amplitude distribution of the volcanic tremor was consistent with the exponential scaling law rather than the power law, suggesting a scale-bound source process. This result suggests that the volcanic tremor originated from a similar physical process occurring practically in the same place. The increment of the tremor amplitude was coincident with the occurrence of impulsive infrasonic waves and vent formations. High-amplitude seismic phases were observed prior to the infrasonic onsets. The time difference between the seismic and infrasonic onsets can be explained assuming a common source located at the vent. This result suggests that both seismic and infrasonic waves are generated when a gas slug bursts at that location. The frequency components of the seismic phases observed just before the infrasonic onset were generally consistent with those of the tremor signals without infrasonic waves. The burst of a gas slug at the surface vent may be a reasonable model for the generation mechanism of the volcanic tremor and the occurrence of impulsive infrasonic signals.

Keywords: Volcanic tremor, Phreatic eruption, Duration-amplitude distribution, Hakone volcano

Background

A volcanic tremor is a continuous seismic signal that lasts minutes to days in duration and is observed during volcanic eruptions or sometimes independently. Most volcanic tremors are represented in a restricted frequency range of 1–9 Hz and with a wide variety of emerging patterns (McNutt 1992). For example, the volcanic tremor prior to the magma eruption at Sakurajima, western Japan (Kamo et al. 1977), represented a clear series of spectral peaks within 1–10 Hz that changed with time, suggesting a resonance of the conduit and temporal changes of the properties of the material within it. On the other hand, volcanic tremors with a period near 15 s were also observed at the Aso volcano; this was related to the resonance of a shallow crack (e.g., Kawakatsu et al. 2000). Aki and Koyanagi (1981) reported that a continuous harmonic tremor under Kilauea, Hawaii, varied with time in relation to the flow of magmatic fluid in a deep magma source. Volcanic tremors were also observed during a phreatic eruption (e.g., Ogiso et al. 2015). The

*Correspondence: yukutake@onken.odawara.kanagawa.jp
[1] Hot Springs Research Institute of Kanagawa Prefectural Government, 586 Iriuda, Odawara, Kanagawa, Japan
Full list of author information is available at the end of the article

duration-amplitude distribution of volcanic tremors is generally described well by an exponential function (e.g., Benoit et al. 2003; Chardot et al. 2015) rather than the power law scaling reported for an ordinal earthquake.

Several generation mechanisms have been proposed for volcanic tremors, although a physical understanding of their origins has been elusive. Julian (1994) proposed a model in which oscillations of the channel were excited by a nonlinear process that occurred when magmatic fluid flowed through it. Chouet (1988) demonstrated that resonance induced in a fluid-filled crack by an impulsive pressure transient could explain many of the observed characteristics associated with long-period events and harmonic tremors. A magma-wagging oscillation against the restoring gas-spring force of the annulus around the magma column was modeled for volcanic tremors during a magma eruption (Jellinek and Bercovici 2011). The growth and collapse of bubbles as groundwater boils is thought to be a reasonable mechanism for harmonic tremors at geysers (Leet 1988). However, volcanic tremors accompanied by a phreatic eruption remain poorly understood. The installation of a dense network of seismic stations near the source of the signal is essential. A small phreatic eruption of the Hakone volcano provided an opportunity to address this issue, because seismic data were measured through such a dense network of stations that were installed near the eruption vents.

The Hakone volcano is located in the northern part of Izu Peninsula, central Japan (Fig. 1). Although there is no historical record of magma eruption, fumarolic activity has persisted in the Owakudani (or Owakidani) geothermal region, approximately 1000 m above sea level on the northern slope of the central cone. Within the caldera, intense swarm activities have often been observed at depths of 0 km (sea level) to 8 km (e.g., Yukutake et al. 2010; Mannen 2003). During these swarm activities, most of the earthquakes reported have been volcano-tectonic (VT) ones generated by the failure of brittle faults. They exhibit a clear onset of *P*- and *S*-waves.

The activity of VT earthquakes in the Hakone volcano gradually increased from the end of April to the end of May 2015 (Fig. 2). The most pronounced activity was observed on May 16, 2015, when more than 1000 VT earthquakes occurred, and the activity gradually decreased beginning in June. The Global Navigation Satellite System detected a stretching of the baseline length across the volcano slightly before the onset of the seismic activity, reflecting an inflation of the pressure source at a depth of around 8 km (Harada et al. 2015). A local ground uplift was also detected using interferometric SAR (InSAR) in Owakudani from the beginning of May (Doke et al. 2015).

An abrupt increase in the number of VT earthquakes occurred in the morning of June 29, 2015 (07:32 on June 29, 2015, JST) (Fig. 2). From 07:32 to 07:34, tilt meters and broadband seismometers around the Owakudani geothermal region detected tilt changes of approximately 10 μ rad (Fig. 1) (Honda et al. 2015). Honda et al. (2015) concluded that these tilt changes could be explained, assuming that a shallow open-crack source approximately

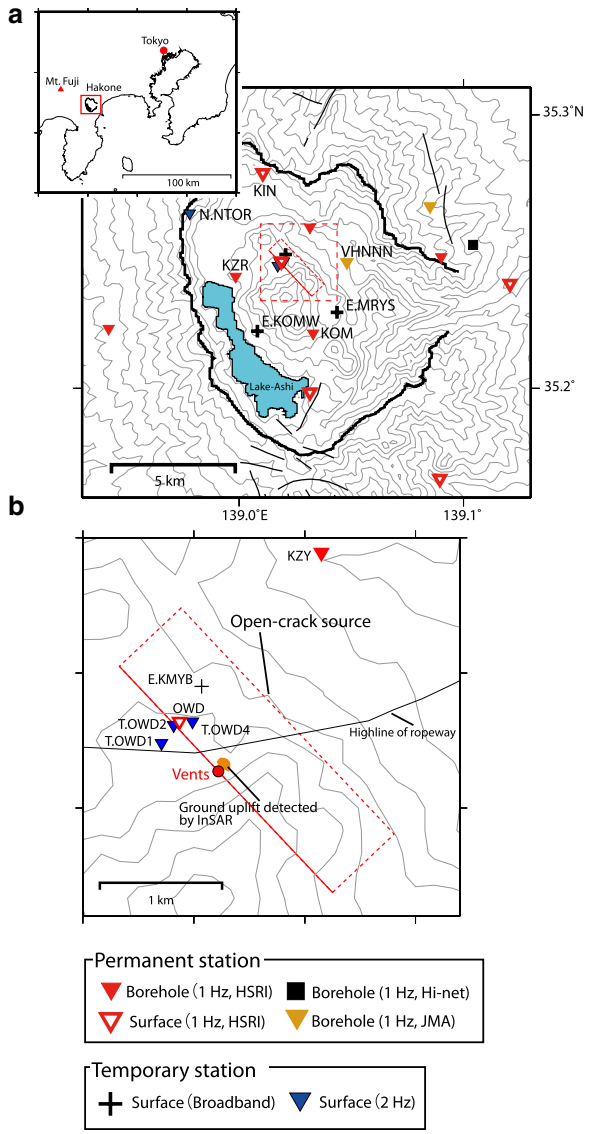

Fig. 1 Maps of Hakone volcano. **a** Distribution of seismic stations in and around the caldera. The study location is indicated by the red rectangle in the inset map. The bold line indicates the rim of the caldera. Gray lines show the detailed topography of Hakone volcano. **b** Magnified map of the area around the Owakudani geothermal region. The red dot indicates the location of the vents that formed during the phreatic eruption (Mannen et al. 2015). The orange region indicates the area of ground uplift detected by SAR interferometry that started 2 months before the eruption (Doke et al. 2015). The red rectangle indicates the location of the open-crack source oriented NW–SE that was estimated by the tilt change (Honda et al. 2015)

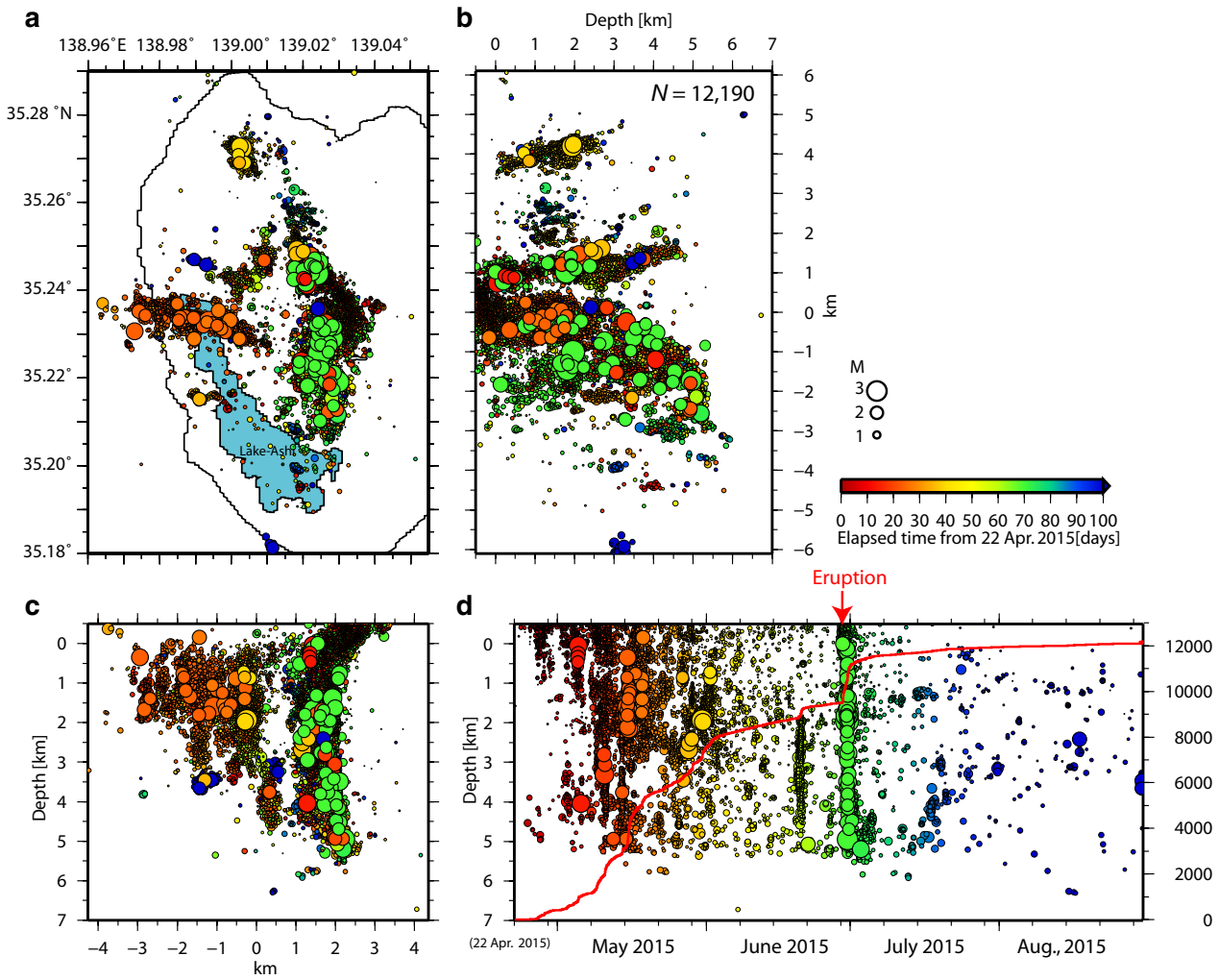

Fig. 2 Hypocenter distribution of VT earthquakes that occurred from April 22 to August 31, 2015. **a** Epicentral distribution, **b** depth distribution along the N–S section, **c** depth distribution along the E–W section, **d** time-depth distribution. The red line indicates the cumulative number of VT earthquakes. The color of each circle indicates the time elapsed from April 22, 2015

5 cm in dilation and oriented NW–SE had expanded to an elevation of approximately 850 m (i.e., several hundred meters below the surface). The open-crack source was also estimated from surface deformations detected by InSAR (Doke et al. 2015). Mannen et al. (2015) reported ash fall in the Owakudani geothermal region around 12:00 on June 29, and several vents were formed there from the afternoon of June 29 until the early morning of July 1. During this phreatic eruption, only 100 tons of altered material that developed near the surface of the steaming area was released (Nagai et al. 2015). The total mass discharged during the eruption was less than 1% of that discharged from the 2014 phreatic eruption of the Ontake volcano, Japan, as estimated by Takarada et al. (2016).

In the present study, we conducted a detailed investigation of the characteristics of the continuous volcanic tremor observed from around 11:00 on June 29 until the early morning of July 1, 2015, including its frequency content, temporal variations in its amplitude, duration-amplitude distribution, and source locations. By comparing these results with other observations, such as the infrasonic waves and vent formation timings, we discuss the generation mechanism of volcanic tremors.

Characteristics of the volcanic tremor

We detected the continuous signals mainly within 1–12 Hz (the frequency range within the white box in Fig. 3a); these are obviously different from the signals generated during VT events (Fig. 4). The energy of the

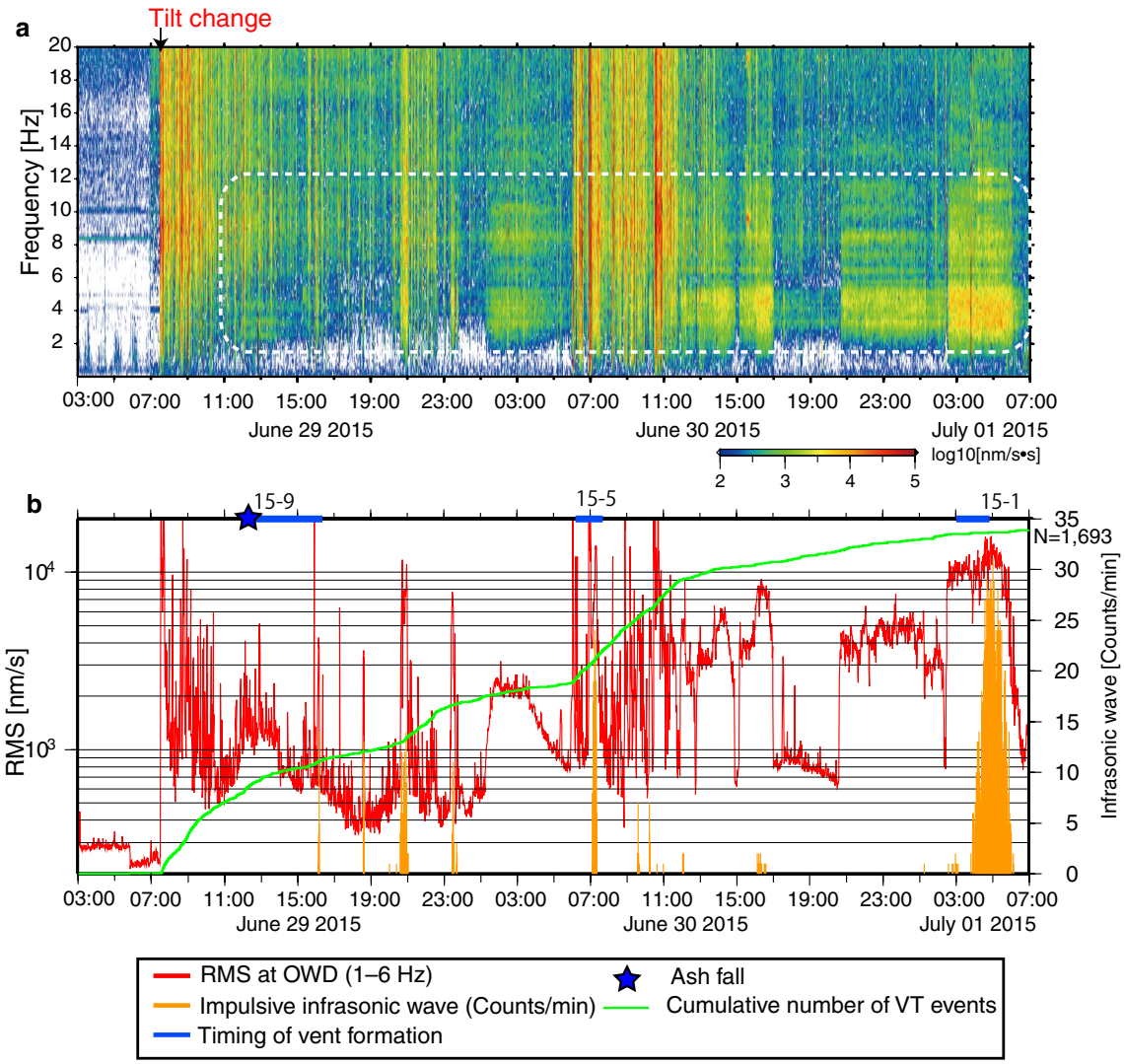

Fig. 3 Seismic record from OWD station during the eruption. **a** Spectrogram of the vertical ground velocity from 3:00 on June 29 to 7:00 (JST) on July 1, calculated by using a 40-s time window with 20-s intervals. The instantaneous increases in amplitude within a wide frequency range correspond to signals from VT earthquakes, whereas the continuous signal within the region framed by the box is due to the volcanic tremor. **b** Root-mean-square amplitude of the filtered vertical ground velocity (1–6 Hz) using a 1-min time window (red line). In order to mitigate contamination by VT earthquakes, signals from earthquakes were deleted using an auto-detection algorithm based on the short-term average/long-term average ratio. The vertical orange lines and horizontal blue bars indicate impulsive infrasonic wave counts per minute and the vent formation times (Mannen et al. 2015), respectively. The numbers on the blue bars show the index number of vents defined in Mannen et al. (2015). The green line indicates the cumulative number of VT events that occurred during this period

seismic signal is particularly concentrated within 1–6 Hz (Fig. 5). The characteristics of the frequency content are generally invariant with time throughout the period (Fig. 3a) and independent of the amplitudes (Fig. 5). The precise time at which the signal began could not be identified due to the overlap of numerous VT events immediately after the tilt change. The signal was observed from at least 11:00 on June 29 until early in the morning of July 1, with its amplitude increasing and decreasing repeatedly. The signal with the highest amplitude was observed at the end of activity, from 03:00 to 06:00 on July 1, and could not be detected thereafter (Fig. 3b). The signal was pronounced at the seismic stations located near the Owakudani region and could not be detected other than during this eruptive activity. Therefore, the signal is assumed to be related to the eruptive activity and can be defined as a volcanic tremor considering its duration and frequency component.

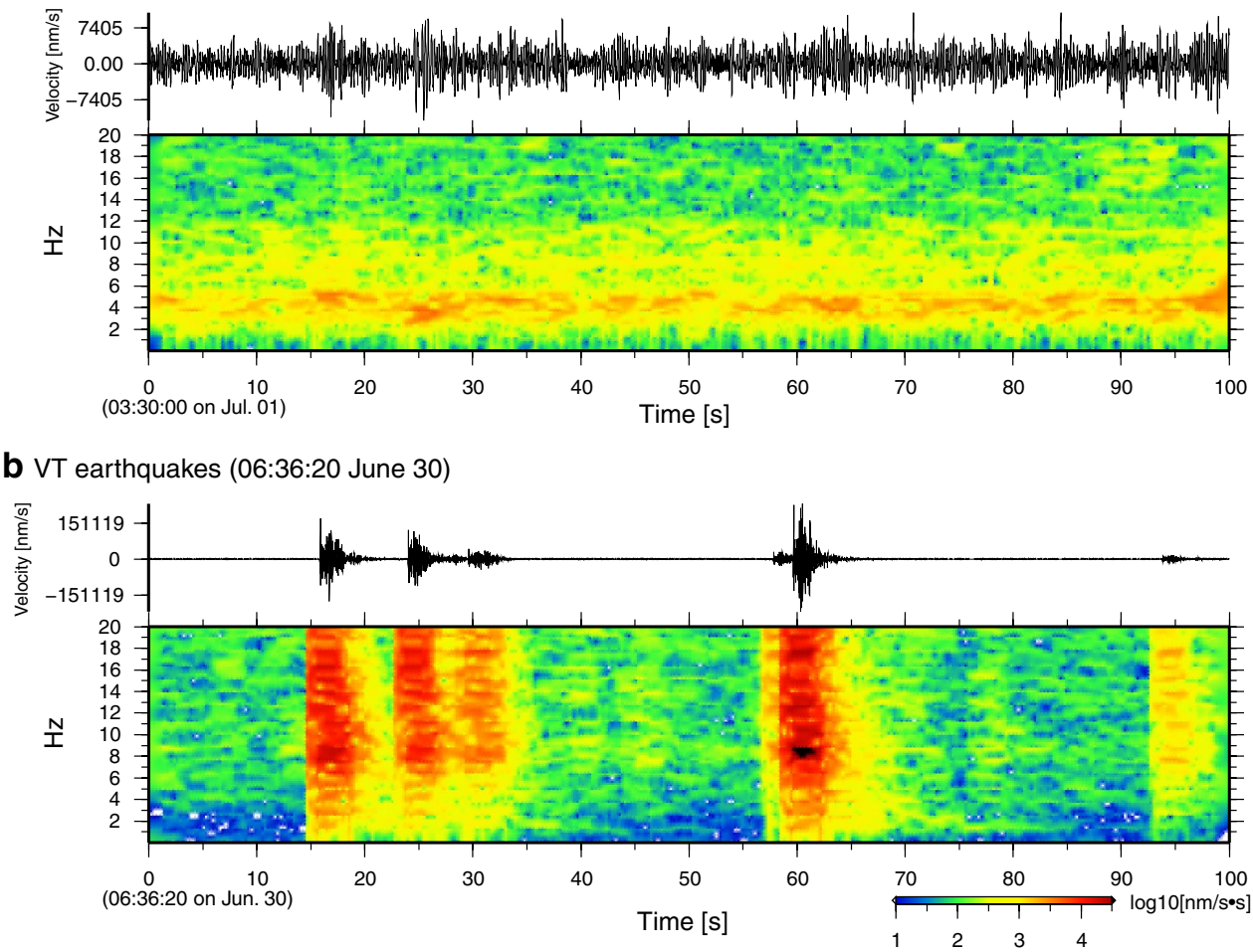

Fig. 4 Examples of the velocity waveforms (vertical component) and spectrograms at OWD station. **a** Volcanic tremor at 03:30:00 on July 1 and **b** VT earthquakes at 06:36:20 on June 30. Each spectrogram was calculated by using a 2.56 s time window with 0.2 s intervals

Data

Twelve permanent seismic stations are operated by the Hot Springs Research Institute, the National Research Institute for Earth Science and Disaster Resilience Hi-net, and the Japan Meteorological Agency (Fig. 1) in and around the caldera of Hakone volcano. Seven of these are borehole-type short-period (1 Hz) seismometers equipped with tilt meters, and the other four are short-period (1 Hz) seismometers on the surface of the ground. In addition to these permanent stations, we set up seven portable seismic stations, including four short-period seismometers (2 Hz) and three broadband (120 s) seismometers, prior to the eruption. All the stations took recordings continuously at a sample rate of 200 Hz for the short-period seismometers and 100 Hz for the broadband seismometers. Consequently, a dense seismic network, including four short-period seismometers and one broadband seismometer (Fig. 1b), developed within 1 km of the vents prior to the eruption. Detailed information on the hypocenter distribution of VT earthquakes (Fig. 2) was obtained based on the seismic data using the double difference (DD) method (Waldhauser and Ellsworth 2000) and the three-dimensional velocity structures estimated by Yukutake et al. (2015).

Determining the location of the source of the volcanic tremor

It was difficult to determine the location of the source of the tremor using the classic method of finding the hypocenter with an inversion of absolute travel times because we could not identify the onset of the body waves. Methods have been developed to locate the source of a tremor

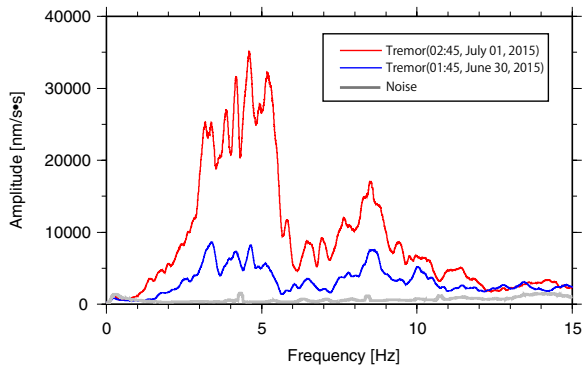

Fig. 5 Examples of amplitude spectra for the vertical ground velocity waveforms at OWD station during the volcanic tremor (blue and red) and the noise record (gray). Each spectrogram was calculated using a waveform of 650 s that was smoothed using a Parzen window with a passband of 0.2 Hz

using seismic amplitudes (e.g., Kumagai et al. 2010; Battaglia and Aki 2003). However, we identified a coherent phase in the volcanic tremor across the stations, instead of *P*- and *S*-wave onsets, via a waveform envelope (Fig. 6). Therefore, we applied a cross-correlation method to obtain the relative arrival time of this coherent phase according to the procedure developed by Obara (2002) for determining the source of a nonvolcanic tremor. Uchida (2014) demonstrated that the envelope correlation method is also useful for determining the signal source for a volcanic tremor.

In the present analysis, the seismic waveform data from 13 stations located within 5 km of the vents, which represent a high signal-to-noise ratio, were used (Fig. 6) after the frequency response of the seismometer was removed. The root-mean-square (RMS) envelope was calculated from the three-component velocity waveforms 1 min in duration. Then, considering the frequency content of the volcanic tremor, we applied a band-pass filter between 2 and 6 Hz and used a 2-s sliding time window to calculate the RMS amplitude. A waveform record with a sample rate of 200 Hz was reduced to 100 Hz. We visually excluded the signals from VT earthquakes if they were contained within a 1-min waveform record. We calculated the cross-correlation coefficients of envelope seismograms across all station pairs by moving the 1-min trace with the lag time of every sampling interval. The lag time with the maximum correlation coefficient was used as the differential arrival time for the coherent signal between two stations. We used only the differential arrival time data with cross-correlations greater than or equal to 0.8.

If differential arrival times meeting the above cross-correlation threshold were obtained for at least 20 station pairs, we then tried to estimate a location for the source of the waveform envelope record. We conducted a grid search at intervals of 100 m, setting the nodes of grids within ± 2 km E–W and N–S and from − 1 to 3 km vertically, centered at the position of the vents. On the vertical axis, 0 km corresponds to sea level and − 1 km corresponds to the elevation at the Owakudani region. We calculated the synthetic arrival time from each grid node to the stations using the three-dimensional velocity structure of the Hakone volcano estimated by Yukutake et al. (2015). The pseudo-bending method (Um and Thurber 1987) was applied to calculate the travel time from a grid node to a station containing its elevation. We assumed that seismic waves detected by the envelopes propagated at *S*-wave velocities. We calculated the residuals at each grid node as the sum of misfits between observed and synthetic differential arrival times for all available pairs and found the best source for the location of the tremor that produced the minimum residual.

Figure 7 shows the results obtained using the grid search method for the seismic records in Fig. 6. The

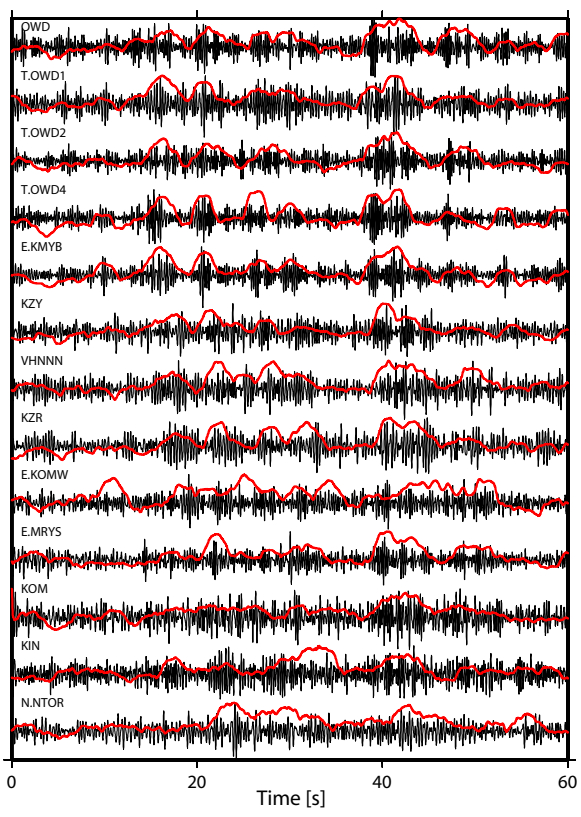

Fig. 6 Example of a 1-min waveform record from each station, taken during the volcanic tremor. Black traces indicate the vertical components of velocity waveforms for the period 2:32:20–2:33:20 on July 1, 2015, to which a band-pass filter between 2 and 6 Hz has been applied. Red traces indicate three-component RMS envelopes for the band-passed signals

best solution was determined to be close to the vents at a depth of − 1 km. To assess the uncertainty regarding the location of the tremor determined using the above procedure, we applied the bootstrap resampling method. The synthetic data set was calculated by adding the randomly resampled final residuals to the synthetic differential arrival times at the best solution. We then applied the same procedure to the synthetic data set and repeated this process 500 times. The results are indicated by gray circles in Fig. 7. The error of the location of the tremor source was defined as double the standard deviation (2σ) of the location shift from the best solution to each bootstrap resampling result. In Fig. 7, the location error was estimated to be 0.4 km in the E–W direction, 0.6 km in the N–S direction, and 0.4 km in the vertical direction.

We also evaluated the validity of the envelope correlation method for determining the location of the tremor source by applying it to a VT earthquake for which the hypocenter could be well constrained. We used the waveform of the VT earthquake that occurred beneath the Owakudani geothermal region at a depth of 0.2 km at 11:12:31 on June 29, 2015. The local magnitude of the event was − 0.6, and the amplitude of the waveform was comparable to that of the volcanic tremor. The locations determined by the two methods differ 0.20 km horizontally and 0.67 km vertically (Fig. 8). The error for the location of the VT event estimated by the bootstrap method was estimated as 0.62 km in the E–W direction, 0.56 km in the N–S direction, and 1.1 km in the vertical direction. The hypocenter obtained by the DD method was included in these location errors (Fig. 8). The results

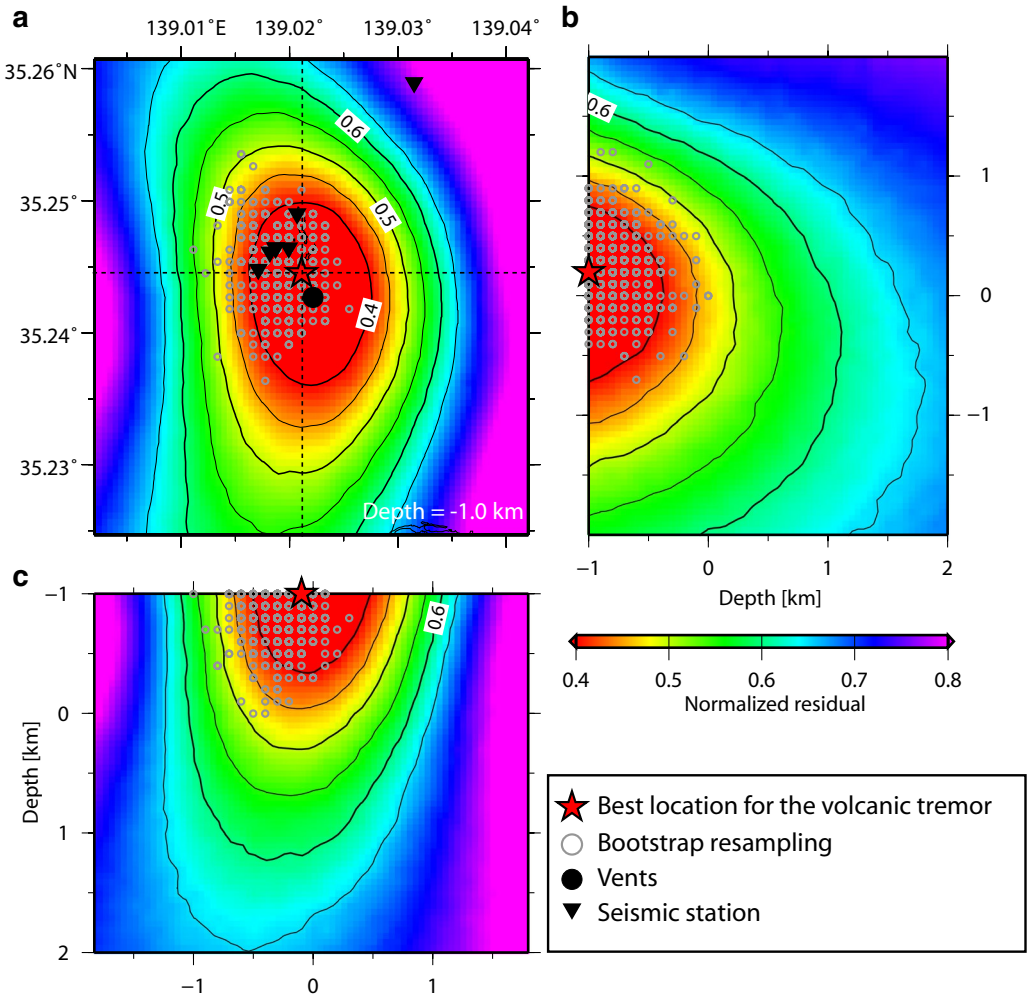

Fig. 7 Result of grid search for the volcanic tremor source in Fig. 6. **a** Epicenter, **b** N–S cross section, and **c** E–W cross section. The red star and gray circles indicate the best location of the tremor source and the results of the bootstrap resampling method, respectively. The colors and contour lines on each diagram show the residual normalized by the maximum value on the section passing through the location of the best solution

indicate that determining the location using the envelope correlation, and the corresponding estimation of uncertainty, is a reliable method.

As a result, we determined the locations of the sources of the volcanic tremors for 19 time windows from 23:38 on June 29 to 06:09 on July 1, for which the location error was less than 0.8 km horizontally and vertically (Fig. 9). The locations of the volcanic tremors are concentrated near the vents. Their sources − 1 km deep; in other words, they are near the surface of the Owakudani geothermal region. On the other hand, the VT earthquakes that occurred during the eruption were distributed at a depth of around 0 km (sea level) (Fig. 9). Considering the location error for the source of the tremor, this difference in depth between the VT earthquakes and the volcanic tremors is significant. The latter occurred around an upper extension of the open crack estimated by the tilt changes (Honda et al. 2015).

Discussion

Validity of the location of the source of the tremor

The particle motion of the volcanic tremor at OWD station (Additional file 1: Figure A1) is a predominately transverse component (*SH* wave). A coherent phase of the volcanic tremor is propagated with apparent velocities of 1.5–2.0 km/s (Additional file 1: Figure A2). The average *P*-wave velocity above sea level within the Hakone caldera estimated in a seismic experiment using explosive sources is 2.76 km/s (Oda 2008), which corresponds to an *S*-wave velocity of 1.60 km/s, assuming a *Vp*/*Vs* ratio of 1.73. Therefore, it is reasonable to assume that the signal of the volcanic tremor was generated near

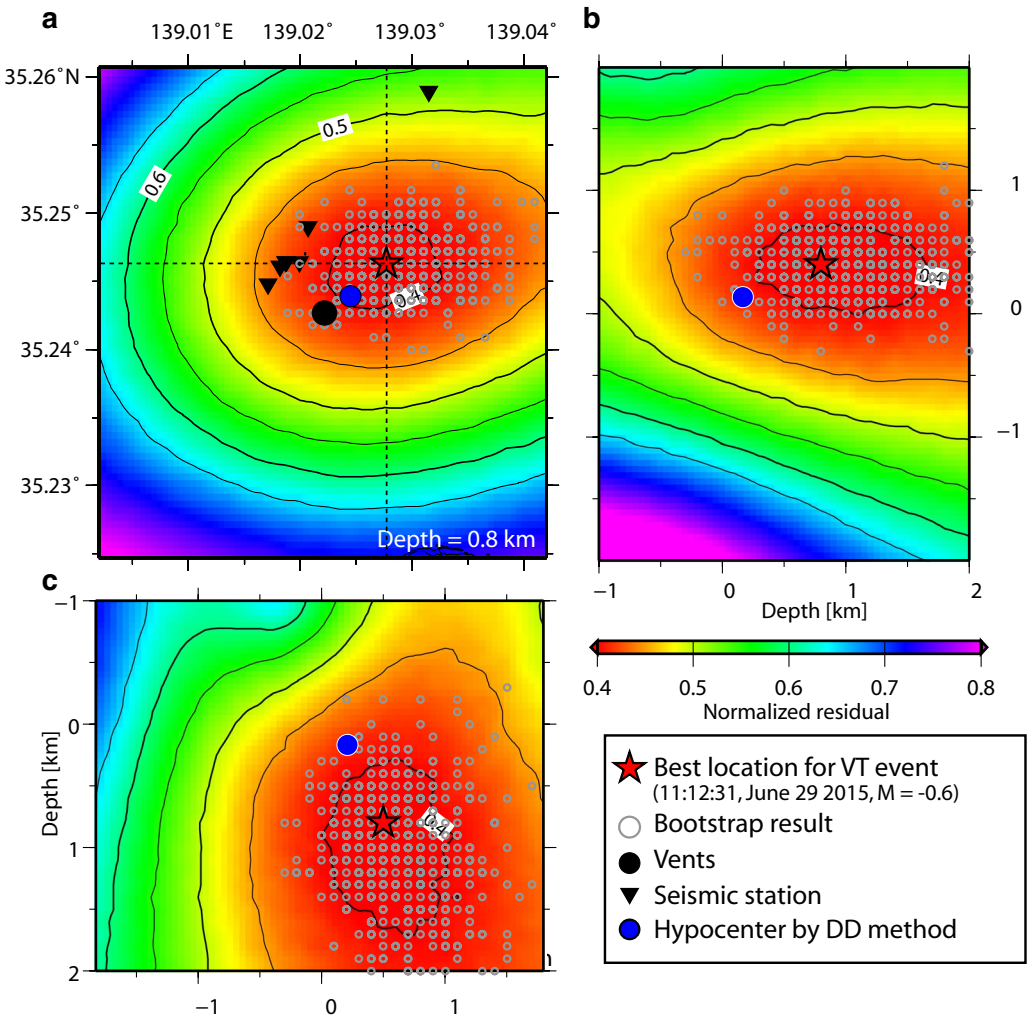

Fig. 8 Result of a grid search for hypocenter of a VT earthquake. **a** Epicenter, **b** N–S cross section, and **c** E–W cross section. The red star and gray circles indicate the best solution for the hypocenter and the results of the bootstrap resampling method, respectively. The blue circle indicates the hypocenter of the VT earthquake as determined using the double difference method

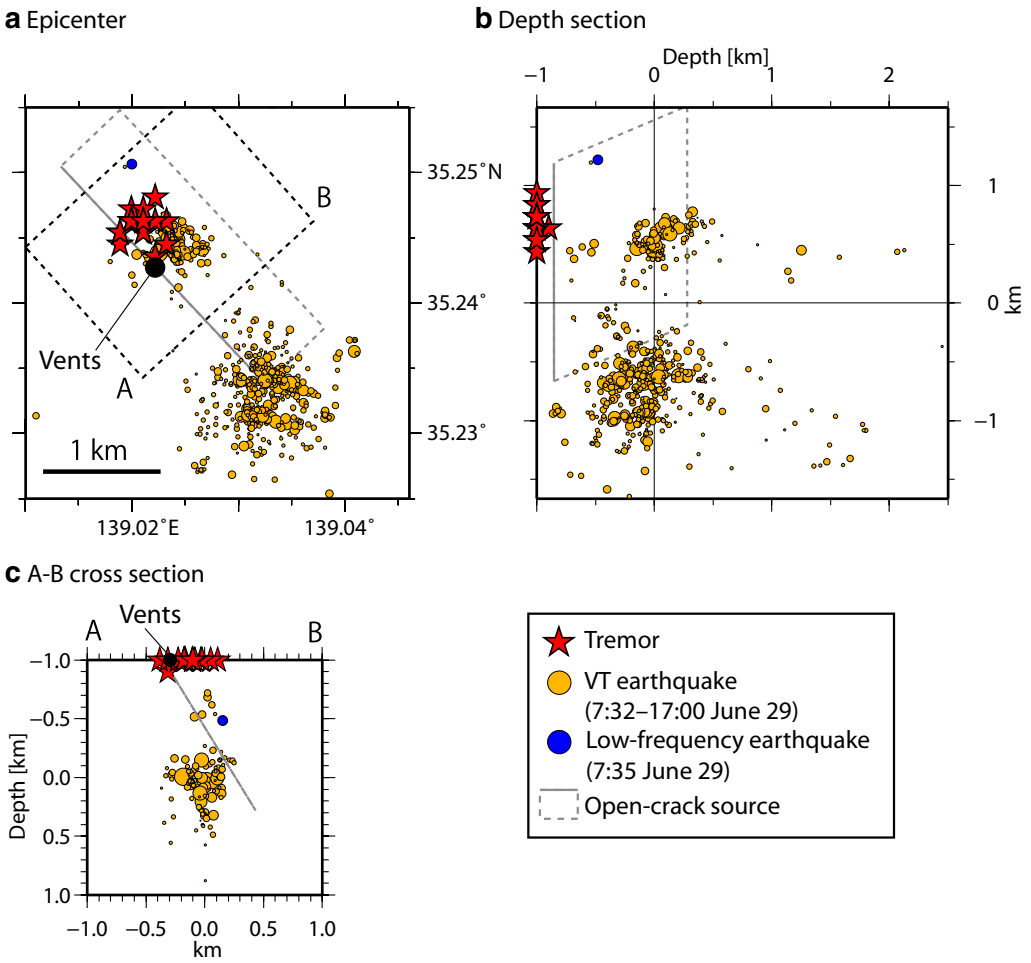

Fig. 9 Locations of the sources of the volcanic tremors. **a** Epicentral distribution, **b** depth section along E–W section, and **c** depth section along A–B section. Red stars indicate the locations of the sources of the tremors, obtained using the envelope correlation method. Orange circles show the hypocenters of VT earthquakes that occurred from 07:32 to 17:00 on June 29, 2015. Blue circles indicate the hypocenters of low-frequency earthquakes. Black circles and gray quadrilaterals represent the locations of vents and the open-crack sources, respectively

the surface and propagated at *S*-wave velocity. This is consistent with the results of grid search (Fig. 7).

Considering the location errors estimated using the bootstrap method, the scattering of the tremor locations in an area with a diameter of approximately 500 m (Fig. 9) may be attributed to errors in the estimation of the location of the source, rather than a true spatial distribution of the source of the tremor. This is supported by the temporal changes seen in the amplitude ratio during the tremor activity (Additional file 2). When the amplitude of volcanic tremor was dominant, the seismic amplitude ratios of E.KMYB and T.OWD1 to OWD station, and E.KMYB to T.OWD1 station, converged to 0.3, 0.2, and 0.7–0.8, respectively. These results suggest that the volcanic tremor originated from a similar physical process occurring at practically the same position.

Duration-amplitude distribution of the volcanic tremor

To discuss the physical processes underlying the volcanic tremor, we investigated its duration-amplitude distribution according to the method reported by Benoit et al. (2003), which corresponds to the frequency-magnitude distribution for an ordinal earthquake. In contrast to the latter, it is difficult to count events of a particular size for a continuous tremor signal. Therefore, we applied a different approach in which the duration of the tremor was used as an analogy for the event count. The waveform from 13:00 on June 29 to 07:00 on July 1, 2015, at the E.KMYB broadband station, which was close to the vents (Fig. 1b), was used to estimate the reduced displacement (Aki and Koyanagi 1981) that accounts for the instrument magnification, distance to source, and type of wave. We removed the signal from VT earthquakes using an auto-detection algorithm based on the short-term

average/long-term average (STA/LTA) ratio. We assumed a body wave and a source located at the vents. The duration of the tremor was measured at a given amplitude of the reduced displacement (or greater), and the relationship between the duration of the tremor and the amplitude was plotted on both log-linear axes and log–log axes (Fig. 10). We fit both power law (log–log) and exponential law (log-linear) models to the duration-amplitude distributions.

The result showed that the exponential model appeared to fit the data better than the power law model (Fig. 10), which is a contrast to the frequency-magnitude distribution for an ordinal earthquake since the latter obeys the power law model. The power law model implies self-similarity of the source process. The exponential duration-amplitude distribution has also been observed for volcanic tremors in several other volcanoes and geothermal regions, suggesting that the tremor-generating process is scale bound (Benoit et al. 2003). Benoit et al. (2003) suggest two possibilities for a scaling bound on the amplitude of the tremor: (1) fixed-source geometry with variable forces that drive the tremor or (2) constant force and variable source geometries. The characteristics of the frequency component that are invariant with time (Fig. 5), concentrated distribution of the tremor sources near the vents (Fig. 9), and time-invariant amplitude ratios (Additional file 2) suggest that the first model is plausible for the volcanic tremor in the present study.

In Fig. 10, λ is the slope of the line or scaling parameter. The inverse of this parameter, λ^{-1}, can be considered the characteristic amplitude of the distribution (Benoit et al. 2003). The characteristic amplitude of 0.11 cm^2 for the tremor in the Hakone volcano is 100 times that of the geothermal noise in the geyser Old Faithful at Yellowstone National Park, Wyoming, in the USA. It is of the same order of magnitude as the noneruptive tremor at Mt. Spurr, Alaska, in the USA, which is interpreted as being of hydrothermal origin, and is one order of magnitude less than that observed during the sub-Plinian eruption at the same volcano. The estimated characteristic amplitude is also of the same order of magnitude as the volcanic explosion earthquakes at Stromboli (Nishimura et al. 2016, 2017), which were related to the behavior of a gas slug in the magma column (e.g., Ripepe and Gordeev 1999).

Relation to vent formation and infrasonic waves

During the eruptive activity, impulsive infrasonic waves were sometimes observed using a microphone installed at OWD station. The occurrence of these appears to accord with the increment of the tremor amplitude. For example, the volcanic tremor with the largest amplitude was observed from 03:00 to 06:00 on July 1, and pronounced impulsive infrasonic wave activity was observed from 04:00 to 06:00 on the same day (Fig. 3). The timing of the vent formation reported by Mannen et al. (2015) also appeared to coincide with the occurrence of the volcanic tremors and impulsive infrasonic waves. The largest vent [15-1 as defined by Mannen et al. (2015)] during the eruption was formed around 04:00 on July 1, based

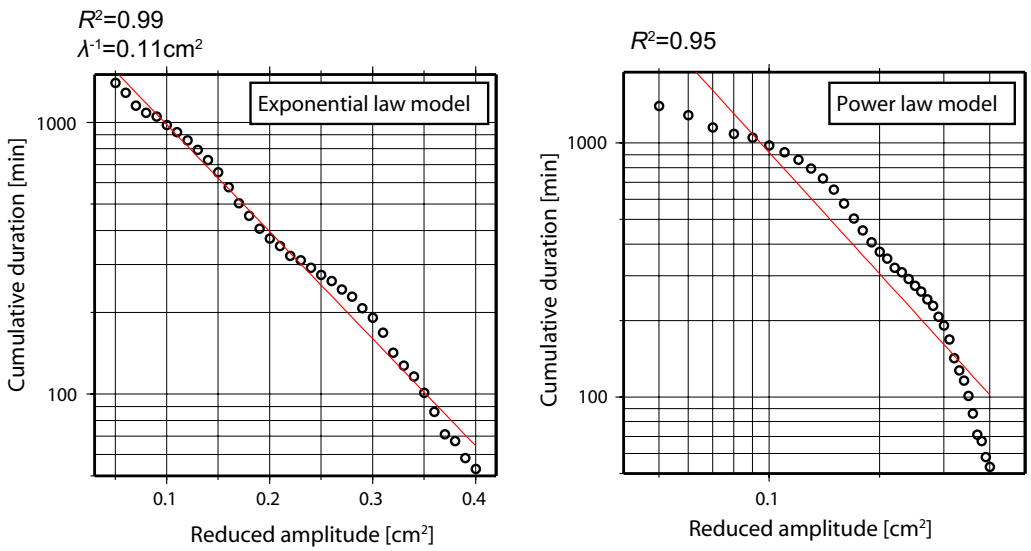

Fig. 10 An exponential model and a power scaling model for the duration-amplitude distribution of the volcanic tremor. The red lines in the diagrams are the least-squares fit of the exponential and power law models. R^2 is the correlation coefficient of the linear regression for both models, and λ^{-1} is the characteristic amplitude of the distribution

on observations with a light-sensitive monitoring camera. There is high uncertainty regarding when the vent formed, due to poor visibility around the Owakudani region during the eruption; however, the timings of two other vent formations, in the afternoon of June 29 (15-9) and around 07:00 on June 30 (15-5), are also coincident with increases in tremor amplitudes and impulsive infrasonic waves (Fig. 3). These observations indicate that tremor activity is sometimes accompanied by impulsive infrasonic waves and vent formation.

Figure 11 shows the seismic and infrasound signals for a period of 100 s starting from 04:05 on July 1, 2015. The impulsive infrasonic signals were observed after 23 s in Fig. 11b. Interestingly, high-amplitude seismic signals within 1–6 Hz occurred immediately before each onset of the impulsive infrasonic signal (e.g., around 70 s in Fig. 11a). Moreover, a high-frequency signal of more than 6 Hz emerged on the vertical velocity waveform coincident with the onset of the infrasonic wave. Figure 12 is a magnified plot of seismic and acoustic records in the time period marked by the red rectangle in Fig. 11a. The time difference (Δt) between onsets of the seismic and infrasonic waves at OWD station was measured as 1.1 s. Since the distance between the vent (15-1) and the station is approximately 520 m (Fig. 1b), the Δt measured can be explained by a source located at the surface of the vent, assuming a sound speed in the air of 340 m/s and

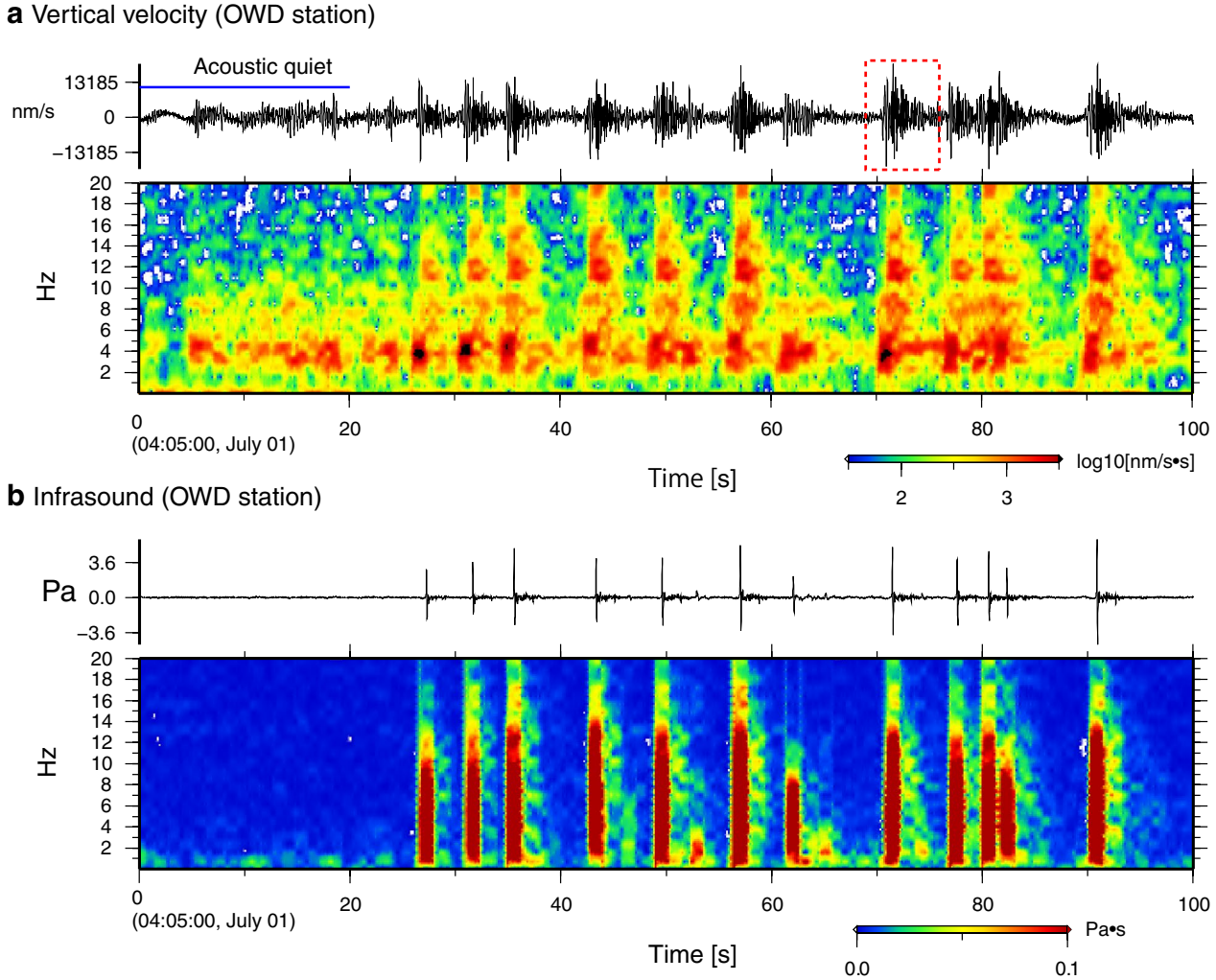

Fig. 11 Vertical velocity and acoustic signals recorded at OWD station during the eruption. **a** The raw seismometer signal (top) and spectrogram (bottom); **b** the raw signal (top) and spectrogram (bottom) from a microphone, for a period of 100 s starting from 04:05 on July 1, 2015. The acoustic signal was corrected using the result of sensor calibration (Yukutake et al. 2017). Each spectrogram was calculated by using a 1.28 s time window with 0.05 s intervals

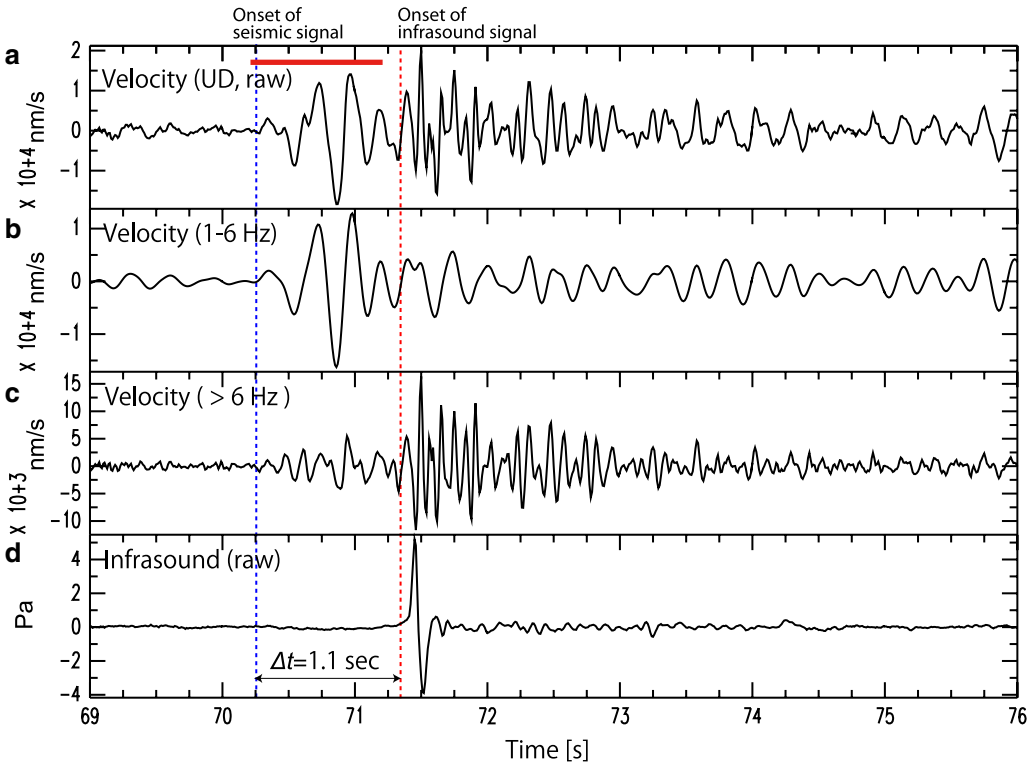

Fig. 12 Magnified plot of seismic and acoustic records within the red rectangle in Fig. 11a. **a**–**c** The raw, band-passed, and high-passed signals of the vertical component of a seismometer. **d** The raw signal of a microphone. The vertical blue and red lines show the onset times for the seismic signal and the impulsive infrasonic wave, respectively

an *S*-wave velocity of 1400 m/s at the surface layer (e.g., Oda 2008).

Similar seismic and infrasonic records were measured during the explosive events at Stromboli (Ripepe et al. 2001). Here the mean Δt, measured as 2.1 s, could not be explained by assuming a common source on the surface of the magma, considering the 300 m between the vent and the station. To explain the large Δt, Ripepe et al. (2001) assumed that the source processes were different, and that the seismic signal was generated by the sudden collapse of foam into a large gas bubble (a gas slug) in the magma column, whereas the infrasound signal was generated by the explosion of a gas slug at the magma surface. The foam collapse model for the generation mechanism of the tremor at Stromboli was supported by the observation of the very-long period (VLP) signals associated with the explosions (e.g., Chouet et al. 1999). On the other hand, the Δt observed at Hakone (Fig. 11) shows that seismic and infrasonic waves are generated at the same time at the surface of the vent. Moreover, we did not observe significant VLP signals exceeding microseismic noise around the infrasonic onsets at the E.KMYB broadband station. Therefore, it is reasonable to consider that the impulsive infrasonic wave and large amplitude seismic signal observed before the infrasonic onset (Fig. 12) were generated by a gas slug bursting at the surface of the vent. The generation of an impulsive infrasonic wave due to a shallow explosive source has been demonstrated by underwater explosion experiments (Ichihara et al. 2009). A similar model was proposed for the tremor activity at White Island, New Zealand (Jolly et al. 2016), in which the dynamic behavior of a gas slug near a surface vent was related to the occurrence of a tremor and infrasonic signals. The high-frequency (> 6 Hz) signal coincident with the infrasonic onset (Fig. 12c) was thought to be produced by a seismic source coupled to the atmosphere, as indicated in Ripepe et al. (2001).

To evaluate the relationship between the seismic signal observed immediately before the infrasonic onset (Fig. 12) and the volcanic tremor during the acoustic quiet period (e.g., 0–20 s in Fig. 11a), we compared the spectrograms of both seismic records (Fig. 13). To exclude contamination by infrasonic waves, we used the 1-s seismogram observed before the infrasonic onset (red line in Fig. 12a). The characteristic of the frequency content for the seismic signal prior to the onset of the infrasonic wave (red line in Fig. 13) is generally consistent with

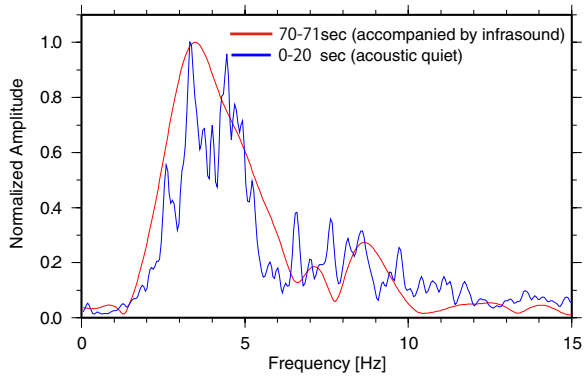

Fig. 13 Comparison of amplitude spectra for the vertical ground velocity waveforms at OWD station. The blue and red lines show the amplitude spectrogram of a seismogram during the acoustic quiet period (indicated by blue line in Fig. 11a) and immediately before the infrasonic onset (indicated by red line in Fig. 12)

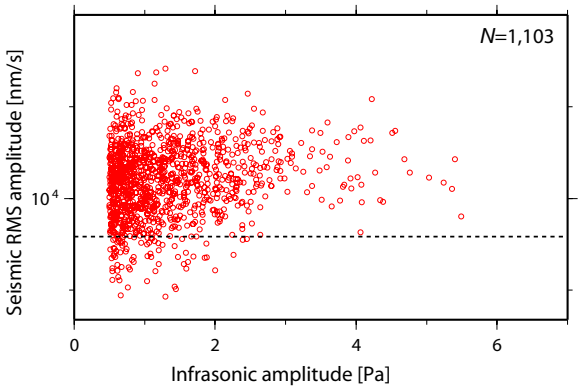

Fig. 14 Relationship between the infrasonic and seismic RMS amplitudes as measured at OWD station. The seismic RMS amplitude was estimated using 1-s three-component velocity waveforms from immediately before the infrasonic onsets that occurred from 04:05 to 05:30 on July 1. The dashed horizontal line indicates the seismic RMS amplitude before the eruptive activity on 04:05:23 on July 1 (time period indicated by the blue line in Fig. 11a)

that for the volcanic tremor without infrasonic signals (Fig. 5 and blue line in Fig. 13). The seismic energy for both signals is concentrated within 1–6 Hz. This result implies that the generation mechanism of both wave fields is more or less the same. Given the result of the envelope correlation analysis (Fig. 9), which determined that the locations of the sources of the volcanic tremors were near the vents and the surface, the bursting of a gas slug at the surface vent could be related to the generation of the tremor signal without infrasonic waves, as well as to the seismic signals prior to the infrasonic onsets.

We investigated the seismic RMS amplitudes within 1–6 Hz 1 s before the infrasonic onsets of 1103 events that occurred from 04:00 to 05:30 on July 1 (Fig. 14). We found that 93% of the impulsive infrasonic signals occurred during large amplitude tremors, which exceeds the amplitude level prior to the eruptive activity on July 1 (seismic RMS amplitude during blue line shown in Fig. 11a). Figure 3b also shows that the RMS amplitudes of the volcanic tremor (1–6 Hz) increased significantly when impulsive infrasonic signals occurred (yellow bars in Fig. 3b). The contamination by infrasonic waves hardly affects the seismic amplitude at this frequency range. This indicates that the infrasonic waves are generated when the amplitude of the volcanic tremor increases.

Candidate mechanism for exciting the tremor

Through the analyses in the present study, we obtained the following results associated with the volcanic tremor: (1) the tremor sources were determined to be near the vents and the surface, (2) the frequency component shows a broad peak within 1–6 Hz that does not vary with time and is independent of the amplitude, (3) the duration-amplitude distribution obeys the exponential scaling law, suggesting a scale-bound source process, (4) the seismic signals prior to the infrasound onsets are related to a gas slug bursting at the surface of the vent, (5) the frequency component with the volcanic tremors during the acoustic quiet period is generally consistent with that of the seismic signal prior to the infrasonic onset, suggesting that the generation mechanism for both seismic signals is basically the same, and (6) the infrasonic waves were generated when the tremor signal increased. Since the source of the volcanic tremor is located around the upper extent of the open crack (Fig. 9) as estimated by Honda et al. (2015), and the signal emerged after the tilt changed (Fig. 3), the tremor activity is also thought to be significantly related to the crack opening.

Considering the above, we propose the following processes as candidate mechanisms for causing the tremor. Small bubbles that form when groundwater boils coalesce into a gas slug that ascends as a slug flow in the channel (Fig. 15a). The boiling of the groundwater in the channel can be attributed to the heat supply that intrudes from the hydrothermal fluid into the open crack. When the gas slug bursts near the surface, the energy that is radiated causes the volcanic tremor (Fig. 15b). Since the characteristics of the frequency content are generally invariant with time throughout the period (Fig. 3a) and is represented by the broad peak around 4 Hz (Fig. 5), it is reasonable to consider that the resonance of the water-filled channel, induced by the energy of the bursting slug, is essential to the generation of the tremor signal. According to Leet (1988), the broad peak observed around 4 Hz corresponds to a channel length of 7–200 m within the range of the speed of sound in water possible

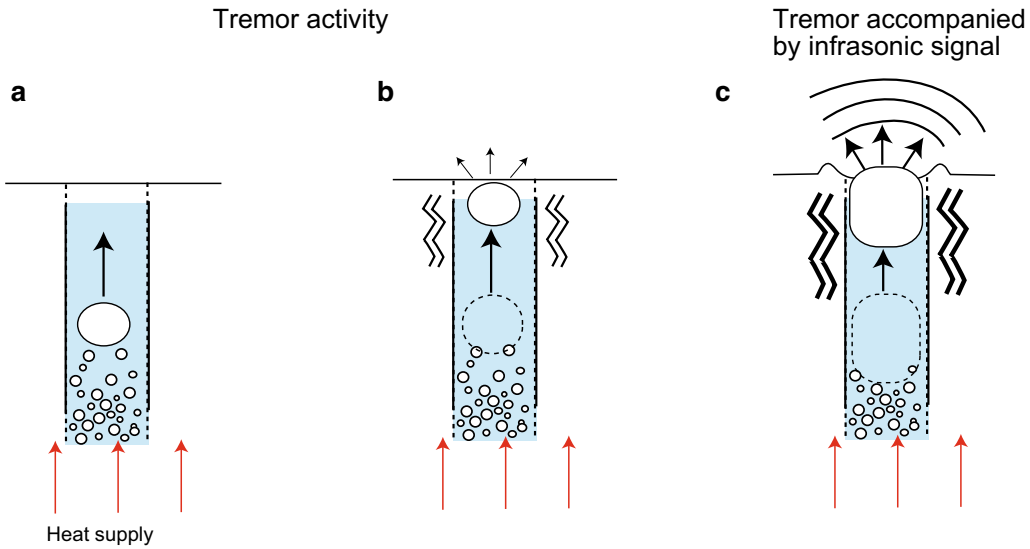

Fig. 15 Schematic diagram of the mechanism that generated the volcanic tremor and the infrasonic signal. **a** and **b** The volcanic tremor during acoustic quiet period, **c** that accompanied by infrasonic signal

at those depths. When a large gas slug is formed in the channel, the bursting slug will be energetic due to the effect of dynamic pressurization near the surface of the liquid (James et al. 2009). In this situation it is expected that significant infrasound signals, accompanied by high-amplitude tremors, will be observed (Fig. 15c). A vent may be formed by repeated energetic bursts. Since burst events occur at a vent at the surface and generate high-amplitude tremors, the time difference between the tremor and infrasonic onsets can be explained by the distance from the vent to the OWD station. High-frequency (> 6 Hz) seismic signals coincident with the infrasonic onset are then generated due to the seismic source being coupled to the atmosphere. The frequency component of the tremor signal should be invariant regardless of the energy released by the bursting slug if parameters such as the sound speed of water within a channel, and the length of the channel, do not change over time.

Conclusions

We investigated, in detail, the characteristics of a volcanic tremor observed 2 days after the phreatic eruption at the Hakone volcano, in the Owakudani geothermal region of central Japan. The frequency component of the volcanic tremor is represented by a broad peak within 1–6 Hz. The characteristics of the frequency component do not vary with time and are independent of the amplitude of the tremor. We estimated the location of the source of the tremor using the envelope correlation method and found that it occurred near eruption vents and at the surface. The duration-amplitude distribution of the volcanic tremor is consistent with the exponential scaling law rather than the power law, suggesting a scale-bound source process. Considering the time-invariant frequency component, concentrated distribution of the tremor source, and time-invariant amplitude ratios, the scaling bound on the amplitude of the tremor suggests a fixed-source geometry with variable forces that drive the tremor. The volcanic tremor likely originated from similar physical processes occurring in practically the same place. The signal of the tremor was sometimes coincident with the occurrence of impulsive infrasonic waves and vent formations. The bursting of a gas slug at the surface of the vent may be a reasonable model with which to explain the generation mechanism of volcanic tremors and the occurrence of impulsive infrasonic signals. The tremor signal is closely correlated to eruptive activity and a useful indicator to assess the status of a hydrothermal system during an eruption.

Additional files

Additional file 1. Example of a waveform, its particle motion, and the apparent velocity of the volcanic tremor. This file shows the particle motion and apparent velocity for the waveform trace of volcanic tremor.

Additional file 2. Temporal changes in amplitude ratios during volcanic tremor. This file shows the temporal changes in the amplitude ratios among the stations near the vents.

Authors' contributions

YY analyzed the data and wrote the manuscript. RH, TU, TS, and SS carried out seismic observations and helped draft the manuscript. RD and MH carried

out seismic observations and processed the data. YM assisted with the data interpretation. All authors read and approved the final manuscript.

Author details
[1] Hot Springs Research Institute of Kanagawa Prefectural Government, 586 Iriuda, Odawara, Kanagawa, Japan. [2] National Research Institute for Earth Science and Disaster Resilience, 3-1 Tennodai, Tsukuba, Ibaraki, Japan. [3] Earthquake Research Institute, The University of Tokyo, 1-1-1 Yayoi, Bunkyo-ku, Tokyo, Japan.

Acknowledgements
We used waveform data from the seismic stations of the National Research Institute for Earth Science and Disaster Resilience, the Japan Meteorological Agency, and the University of Tokyo. We used data obtained from the microphone installed by the Japan Meteorological Agency. We would like to thank Dr. Mie Ichihara for her important suggestions relating to tremor and infrasonic source processes. Dr. Akihiko Terada provided useful comments on geothermal activity during a phreatic eruption. We also thank Dr. Yuki Abe for helpful comments. Yoshiko Teguri supported the data processing for the impulsive infrasonic waves. The code used to calculate the spectrogram was provided by Dr. Yorihiko Osaki. We are thankful to two anonymous reviewers and Editor Diana Roman who helped us to greatly improve this manuscript.

Competing interests
The authors declare that they have no competing interests.

Availability of data and materials
The data that support the findings of this study are available on request from the corresponding author.

Funding
This study was supported by a Grant-in-Aid for Young Scientists (B) (JSPS KAKENHI No. 15K17755).

Publisher's Note

Received: 12 July 2017 Accepted: 27 November 2017
Published online: 06 December 2017

References

Aki K, Koyanagi R (1981) Deep volcanic tremor and magma ascent mechanism under Kilauea, Hawaii. J Geophys Res Solid Earth 86(B8):7095–7109. https://doi.org/10.1029/JB086iB08p07095

Battaglia J, Aki K (2003) Location of seismic events and eruptive fissures on the Piton de la Fournaise volcano using seismic amplitudes. J Geophys Res Solid Earth. https://doi.org/10.1029/2002JB002193

Benoit JP, McNutt SR, Barboza V (2003) Duration-amplitude distribution of volcanic tremor. J Geophys Res Solid Earth. https://doi.org/10.1029/2001JB001520

Chardot L, Jolly AD, Kennedy B, Fournier N, Sherburn S (2015) Using volcanic tremor for eruption forecasting at White Island volcano (Whakaari), New Zealand. J Volcanol Geotherm Res 302:11–23. https://doi.org/10.1016/j.jvolgeores.2015.06.001

Chouet B (1988) Resonance of a fluid-driven crack: radiation properties and implications for the source of long-period events and harmonic tremor. J Geophys Res Solid Earth 93(B5):4375–4400. https://doi.org/10.1029/JB093iB05p04375

Chouet B, Saccorotti G, Dawson P, Martini M, Scarpa R, De Luca G, Milana G, Cattaneo M (1999) Broadband measurements of the sources of explosions at Stromboli Volcano, Italy. Geophys Res Lett 26(13):1937–1940. https://doi.org/10.1029/1999GL900400

Doke R, Harada M, Takenaka J, Mannen K (2015) Surface deformation at Owakudani associated with 2015 volcanic activities of Hakone volcano. Abstracts of the Volcanological Society of Japan 2015 Fall Meeting: A3-13 **(in Japanese)**

Harada M, Doke R, Honda R, Yukutake Y, Itadera K, Mannen K, Takenaka J, Satomura M, Miyaoka K (2015) Crustal deformation and its deformation source associated with volcanic activity of Hakone volcano (2015). Abstracts of the Volcanological Society of Japan 2015 Fall Meeting: P95 **(in Japanese)**

Honda R, Yukutake Y, Harada M, Kato K, Uhira K, Morita Y, Sakai S (2015) Tilt changes and volcanic tremor observed prior to a small eruption of Hakone in 29 June, 2015. Abstracts of the Volcanological Society of Japan 2015 Fall Meeting: P48 **(in Japanese)**

Ichihara M, Ripepe M, Goto A, Oshima H, Aoyama H, Iguchi M, Tanaka K, Taniguchi H (2009) Airwaves generated by an underwater explosion: Implications for volcanic infrasound. J Geophys Res Solid Earth. https://doi.org/10.1029/2008JB005792

James MR, Lane SJ, Wilson L, Corder SB (2009) Degassing at low magma-viscosity volcanoes: quantifying the transition between passive bubble-burst and Strombolian eruption. J Volcanol Geotherm Res 180(2):81–88. https://doi.org/10.1016/j.jvolgeores.2008.09.002

Jellinek AM, Bercovici D (2011) Seismic tremors and magma wagging during explosive volcanism. Nature 470(7335):522–525. http://www.nature.com/nature/journal/v470/n7335/abs/10.1038-nature09828-unlocked.html#supplementary-information

Jolly A, Kennedy B, Edwards M, Jousset P, Scheu B (2016) Infrasound tremor from bubble burst eruptions in the viscous shallow crater lake of White Island, New Zealand, and its implications for interpreting volcanic source processes. J Volcanol Geotherm Res 327:585–603. https://doi.org/10.1016/j.jvolgeores.2016.08.010

Julian BR (1994) Volcanic tremor: nonlinear excitation by fluid flow. J Geophys Res Solid Earth 99(B6):11859–11877. https://doi.org/10.1029/93JB03129

Kamo K, Furuzawa T, Akamatsu J (1977) Some natures of volcanic microtremors at the Sakura-jima volcano. Bull Volcanol Soc Jpn 22:41–58 **(in Japanese with English abstract)**

Kawakatsu H, Kaneshima S, Matsubayashi H, Ohminato T, Sudo Y, Tsutsui T, Uhira K, Yamasato H, Ito H, Legrand D (2000) Aso94: Aso seismic observation with broadband instruments. J Volcanol Geotherm Res 101(1):129–154. https://doi.org/10.1016/S0377-0273(00)00166-9

Kumagai H, Nakano M, Maeda T, Yepes H, Palacios P, Ruiz M, Arrais S, Vaca M, Molina I, Yamashima T (2010) Broadband seismic monitoring of active volcanoes using deterministic and stochastic approaches. J Geophys Res Solid Earth. https://doi.org/10.1029/2009JB006889

Leet RC (1988) Saturated and subcooled hydrothermal boiling in groundwater flow channels as a source of harmonic tremor. J Geophys Res Solid Earth 93(B5):4835–4849. https://doi.org/10.1029/JB093iB05p04835

Mannen K (2003) A re-examination of Hakone earthquake swarms by literature (1917–60): implications for the regional tectonics. Bull Volcanol Soc Jpn 48(6):425–443 **(in Japanese with English abstract)**

Mannen K, Doke R, Harada M, Honda R, Itadera K, Kikugawa G, Yukutake Y, Takenaka J (2015) Chronology of the 2015 eruption of Hakone volcano, Japan. Abstracts of the Volcanological Society of Japan 2015 Fall Meeting: A3-12 **(in Japanese)**

McNutt SR (1992) Volcanic tremor. Encycl Earth Syst Sci 4:417–425

Nagai M, Miwa T, Mannen K, Ishizuka Y, Yamasaki S, Furukawa R, Yoshimoto M, Tsunematsu K, Uchiyama T, Baba A, Suzuki Y (2015) The craters of the 2015 eruption of Hakone volcano, Japan. Abstracts of the Volcanological Society of Japan 2015 Fall Meeting: A3-14 **(in Japanese)**

Nishimura T, Iguchi M, Hendrasto M, Aoyama H, Yamada T, Ripepe M, Genco R (2016) Magnitude–frequency distribution of volcanic explosion earthquakes. Earth Planets Space 68(1):125. https://doi.org/10.1186/s40623-016-0505-2

Nishimura T, Iguchi M, Hendrasto M, Aoyama H, Yamada T, Ripepe M, Genco R (2017) Correction to: magnitude–frequency distribution of volcanic explosion earthquakes. Earth Planets Space 69(1):143. https://doi.org/10.1186/s40623-017-0728-x

Obara K (2002) Nonvolcanic deep tremor associated with subduction in Southwest Japan. Science 296(5573):1679–1681. https://doi.org/10.1126/science.1070378

Oda Y (2008) Seismic velocity structure beneath Hakone volcano. Res Rep Kanagawa Prefect Museum Nat His 13:171–186 **(in Japanese with English abstract)**

Ogiso M, Matsubayashi H, Yamamoto T (2015) Descent of tremor source locations before the 2014 phreatic eruption of Ontake volcano, Japan. Earth Planets Space 67(1):206. https://doi.org/10.1186/s40623-015-0376-y

Ripepe M, Gordeev E (1999) Gas bubble dynamics model for shallow volcanic tremor at Stromboli. J Geophys Res Solid Earth 104(B5):10639–10654. https://doi.org/10.1029/98JB02734

Ripepe M, Ciliberto S, Della Schiava M (2001) Time constraints for modeling source dynamics of volcanic explosions at Stromboli. J Geophys Res Solid Earth 106(B5):8713–8727. https://doi.org/10.1029/2000JB900374

Takarada S, Oikawa T, Furukawa R, Hoshizumi H, Ji Itoh, Geshi N, Miyagi I (2016) Estimation of total discharged mass from the phreatic eruption of Ontake Volcano, central Japan, on September 27, 2014. Earth Planets Space 68(1):138. https://doi.org/10.1186/s40623-016-0511-4

Uchida H (2014) Hypocenter distribution and source mechanism of B-type earthquakes at Miyakejima volcano. Doctoral Thesis, Tohoku University

Um J, Thurber C (1987) A fast algorithm for two-point seismic ray tracing. Bull Seismol Soc Am 77(3):972–986

Waldhauser F, Ellsworth WL (2000) A double-difference earthquake location algorithm: method and application to the Northern Hayward Fault, California. Bull Seismol Soc Am 90(6):1353–1368. https://doi.org/10.1785/0120000006

Yukutake Y, Tanada T, Honda R, Harada M, Ito H, Yoshida A (2010) Fine fracture structures in the geothermal region of Hakone volcano, revealed by well-resolved earthquake hypocenters and focal mechanisms. Tectonophysics 489(1–4):104–118. https://doi.org/10.1016/j.tecto.2010.04.012

Yukutake Y, Honda R, Harada M, Arai R, Matsubara M (2015) A magma-hydrothermal system beneath Hakone volcano, central Japan, revealed by highly resolved velocity structures. J Geophys Res Solid Earth 120(5):3293–3308. https://doi.org/10.1002/2014jb011856

Yukutake Y, Ichihara M, Honda R (2017) Cross-correlation analysis of infrasound and seismic signal during the phreatic eruption at Hakone in 2015. Abstracts of Japan Geoscience Union Meeting 2017: SVC47-P10